RSC Advances

PAPER

View Article Online
View Journal | View Issue



Cite this: *RSC Adv.*, 2020, **10**, 11371

# Microwave assisted green synthesis of $Fe_2O_3$/biochar for ultrasonic removal of nonsteroidal anti-inflammatory pharmaceuticals

Zakaria Anfar, [ab] Mohamed Zbair, *[c] Hassan Ait Ahsiane, *[de] Amane Jada[b] and Noureddine El Alem[a]

Received 20th January 2020
Accepted 10th March 2020

DOI: 10.1039/d0ra00617c

rsc.li/rsc-advances

Iron oxide/biochar ($Fe_2O_3$/biochar) was prepared by green synthesis *via* a microwave to evaluate ultrasound-assisted adsorption capacity of Nonsteroidal Anti-inflammatory Drugs (NSAIDs) (salicylic acid, naproxen, and ketoprofen) from the water. Several techniques of characterization, including, Fourier transform infrared spectrometry, scanning electron microscopy, EDS analysis, $N_2$ adsorption–desorption, X-ray diffraction, and Raman spectrometry were applied. The adsorption of NSAIDs onto $Fe_2O_3$/biochar was performed using an ultrasonic bath. The effects of batch adsorption under various experimental parameters such as contact time (0–120 min), initial concentration (10–500 mg $L^{-1}$) and pH (2–12) were tested. The obtained $Fe_2O_3$/biochar specific surface area, mesopore volume/micropore volume, and pores size were equal to 786 $m^2$ $g^{-1}$, 0.409 $cm^3$ $g^{-1}$, and 1.534 $cm^3$ $g^{-1}$, respectively. The pseudo-second-order model could describe better all NSAID adsorptions onto $Fe_2O_3$/biochar. The Langmuir model agreed well with the NSAID adsorptions and the maximum adsorption capacities reached 683 mg $g^{-1}$, 533 mg $g^{-1}$ and 444 mg $g^{-1}$ for salicylic acid, naproxen, and ketoprofen, respectively. $Fe_2O_3$/biochar can be used as an excellent adsorbent for the treatment of NSAIDs in water.

## 1 Introduction

Currently, it is becoming more obvious that pharmaceutical drugs constitute a gathering of new organic emerging pollutants, which are ceaselessly brought into the water because of their broad medical utilization and ineffective expulsion in wastewater treatment plants (WWTPs).[1] Several studies stated that pharmaceutical compounds and their metabolites are generally identified in wastewater, sewage, surface water, groundwater and even drinking water with a concentration range from nano-gram per liter (ng $L^{-1}$) to microgram per liter (μg $L^{-1}$).[2]

Among these, indomethacin, ibuprofen, ketoprofen, naproxen, diclofenac, and ketoprofen, categorized as non-steroidal anti-inflammatory drugs (NSAIDs), share certain analgesic and antipyretic properties and, due to their high annual consumption, present important research concern worldwide.[1,3] The presence of these compounds (NSAIDs) has been detected in surface and drinking water concentrations going from <0.1 ng $L^{-1}$ to few hundreds of ng $L^{-1}$.[4–6] Hence, it is not easy for the conventional water treatment plants to totally eliminate NSAIDs from water.[7]

Accordingly, some alternative approaches have already been explored for the removal or degradation of NSAIDs,[8] as well as adsorption, electrochemical oxidation, photo-degradation, ultrasonic irradiation, and advanced oxidation process.[9–17] However, adsorption has been found to be the most appropriate technology due to its low-cost, exactitude, feasibility, the simplicity, and safety of the treatment process.[18–25] Moreover, a number of adsorbents such as functionalized carbon nanotubes (FCN), graphene, polystyrene-divinylbenzene resin, activated carbon, and *etc.* have been employed to remove the pharmaceutical drugs from water.[9,26–28]

Besides, searching for new proficient, simple and cheap method to control NSAIDs is also of huge interest. Currently, biochar-based materials have been widely studied in the environmental remediation because of its intrinsic characteristics:[29,30]

- Biochar is cheap, non-toxic and easy to obtain,
- Biochar has inherent high specific surface areas, large pore volumes, allowing the chance of physisorption and hydrophobic interaction and electrostatic adsorption with contaminants proficiently.
- Biochar can be modified and have an increasing quantity of oxygen functional groups on the surface, which permitting the

[a]*Laboratoire Matériaux et Environnement LME, Faculté des Sciences, Université Ibn Zohr, BP 8106, Cité Dakhla, Agadir, Morocco*

[b]*Institute of Materials Science of Mulhouse, Haute Alsace University, Mulhouse, 68100, France*

[c]*Laboratoire de Catalyse et Corrosion des Matériaux, Faculté des Sciences El Jadida, Université Chouaïb Doukkali, BP 20, El Jadida 24000, Morocco*

[d]*Chemical and Biochemical Sciences, Mohammed VI Polytechnic University, Lot 660-Hay Moulay Rachid, Ben Guerir, Morocco. E-mail: hassan.aitahsaine@um6p.ma*

[e]*Laboratoire de Chimie Appliqueé des Matériaux, Centre des Sciences des Matériaux Science Center, Faculty of Sciences, Mohammed V University, Rabat, Morocco*

possibility of particular binding (*e.g.*, hydrogen bonding, π–π electron-donor–acceptor interactions and also covalent binding) for toxins efficiently.

Henceforth, to improve the adsorption effect of biochar, the modification was necessary to improve its surface properties.

Recently, several paper were published about the modification of biochar surface such as: ZnO,[31] $WO_3$,[32] Mg/Al,[33] Ni/Mn,[33] Mg/Fe,[33] amino groups (polyethylenimine),[34] oxygen functional groups (β-cyclodextrin–chitosan)[35] and *etc.* The outcomes of these published paper suggest that functionalization of biochar might intensely develop its adsorption ability. Additionally, these studies point out that the surface and physicochemical properties of biochar can be simply modified with functional groups or incorporated with zinc and/or iron, exhibiting improved physical or chemical properties for the removal of harmful contaminants.

Henceforth, the aim of this research was to (i) synthesis and characterize iron oxide/biochar, (ii) study the removal efficiency of NSAIDs (salicylic acid, naproxen, and ketoprofen) and investigate the impacts of some key parameters, namely pH, concentration and contact time on the adsorption capacity using ultrasonic bath.

## 2 Methods and materials

### 2.1. Materials

The walnut shell (WS) was collected from the southwestern of Morocco (Taroudant city). The walnut shell (WS) was washed with tap water and distilled water. The washed walnut shell (WS) was oven dried at 60 °C for 12 h. The iron precursor was ferric chloride ($FeCl_3 \cdot 6H_2O$) and was purchased from Merck Millipore. Salicylic acid (SA), naproxen (Nap), and ketoprofen (Keto) were acquired from Sigma-Aldrich. Moreover, pH values of the solutions were controlled with HCl (Merck Millipore) and NaOH (Merck Millipore) solutions. All chemicals were used as received and all solutions were prepared with distilled water. The synthesis was performed in a Teflon autoclave using microwave radiation (Delonghi EMD MW 311 adjustable power < 800 W, 230 V, 50 Hz).

### 2.2. Synthesis of $Fe_2O_3$/biochar

Firstly, walnut shell (WS) was mixed with 50 mL of $FeCl_3 \cdot 6H_2O$ ($WS/FeCl_3 = 0.5$) and put into Teflon autoclave. Then, the mixture was heated for 15 min under microwave radiation 280 W. The obtained material was loaded in a quartz reactor and pyrolyzed under an $N_2$ atmosphere (50 mL $min^{-1}$) at 600 °C for 2 hours. Finally, the sample was rinsed with distilled water and dried at 105 °C. The obtained sample was labeled $Fe_2O_3$/biochar. Scheme 1 illustrates the synthesis route of the labeled iron oxide/biochar composite.

### 2.3. Batch adsorption experiments

The adsorption of SA, Nap, and Keto onto $Fe_2O_3$/biochar were performed using an ultrasonic bath. About, 20 mg of $Fe_2O_3$/biochar was added into 100 mL of the SA, Nap, and Keto with known concentration under various experimental parameters

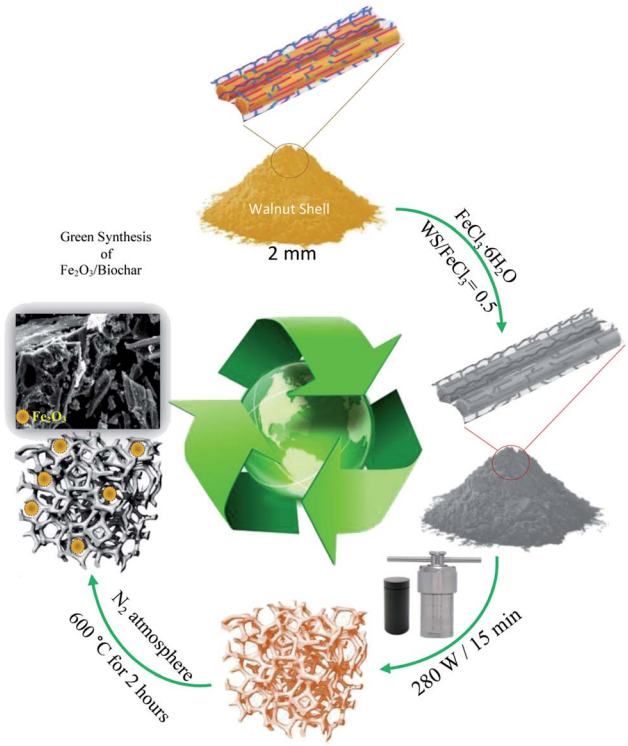


Scheme 1 Synthesis steps of the $Fe_2O_3$/biochar adsorbent.

such as contact time (0–120 min), initial concentration (10–500 mg $L^{-1}$) and pH (2–12). All adsorption experiments were conducted using an ultrasonic bath with the heating system (PS-30A, Ultrasonic Cleaner) at 40 kHz of frequency and 180 W of power. After a suitable time, a portion of the samples was collected from the beakers and filtered. The concentration of SA, Nap, and Keto were determined using a UV-vis spectrophotometer (Shimadzu, 84000S) at an absorbance wavelength of 294.4, 262, and 277 nm, respectively. Table 1 highlights the mathematical models using in this work to fit the data.

### 2.4. Regeneration

The renewability and reusability and of $Fe_2O_3$/biochar, regeneration experiments were carried out by washing the $Fe_2O_3$/biochar after adsorption with ethanol for 4 hours of stirring. Then, sonicated for 15 min, and finally filtered, washed with distilled water and then dried at 110 °C. Five cycles of adsorption-regeneration studies were carried out accordingly.

### 2.5. Characterization

Raman spectroscopy was used to characterize $Fe_2O_3$/biochar using a spectrometer NRS-5100 model Jasco Raman spectrometer and a CCD detector, laser line of 532 nm and objective lens 100×, with a laser power of 1.6 mW. Surface area ($S_{BET}$) of $Fe_2O_3$/biochar after and before adsorption of toxic pollutants was measured using an AUTOSORB-1 and pore size analyzer at 77 K. The Fourier transform infrared spectra of $Fe_2O_3$/biochar was obtained in the mid-infrared region (400–4000 $cm^{-1}$) using a Shimadzu 4800S. The spectra were scanned at a resolution of

 

Table 1 Mathematical models using in this work to fit the data

| Equations | Utility | Description | Ref. |
|---|---|---|---|
| $Q_{e,t} = \frac{(C_0 - C_{e,t}) \times V}{m}$ | Adsorption capacity | $C_0$ (mg $L^{-1}$) and $C_{e,t}$ (mg $L^{-1}$) are the initial and equilibrium concentrations, respectively. $m$ (g) is the weight of adsorbent and $V$ (L) is the volume of adsorbate | 36 |
| $R\ (\%) = \left(\frac{C_0 - C_{e,t}}{C_0}\right) \times 100$ | Removal efficiency | | 37 |
| $Q_t = Q_{cal}(1 - \exp^{K_1 t})$ | Pseudo-first-order | $Q_e$ and $Q_t$ are the adsorbed adsorbate amounts at equilibrium and at times $t$, respectively. $K_1$: the rate constant; $K_2$: rate constant | 38 |
| $Q_t = \frac{(K_2 {Q_{cal}}^2 t)}{(1 + K_2 Q_{cal} t)}$ | Pseudo-second-order | | 39 |
| $Q_t = K_{ip} t^{\frac{1}{2}} + C$ | Intraparticle diffusion | $K_{ip}$ (mg $g^{-1}$ $min^{-1/2}$): rate coefficient; $C$: thickness of the boundary layer | 40 |
| $Q_e = \frac{Q_m K_L C_e}{1 + K_L C_e}$ | Langmuir isotherm | $K_L$: direct measure of the intensity of the adsorption process; $Q_m$: maximum adsorption capacity | 41 |
| $Q_e = K_F C_e^{\frac{1}{n}}$ | Freundlich isotherm | $K_F$: adsorption capacity; $n$: intensity of adsorption; $1/n = 0$ irreversible; $1/n > 1$ unfavorable $0 < 1/n < 1$ favorable | 42 |

2.0 $cm^{-1}$ and with 30 scanning. Scanning electron microscopy (SEM) of $Fe_2O_3$/biochar was analyzed using FEI, Quanta 200-ESEM operated at 20 kV.

# 3 Results and discussions

## 3.1. Characterization

$N_2$-physisorption isotherm of $Fe_2O_3$/biochar exhibit type IV with a hysteresis loop according to IUPAC classification.[43] The calculated textural parameters: specific surface area ($S_{BET}$), mesopores volume, micropores volume, and pores size were equal to 786 $m^2$ $g^{-1}$, 0.409 $cm^3$ $g^{-1}$, 1.534 $cm^3$ $g^{-1}$, and 4.6 nm (Fig. 1a). Fig. 1b presents the FTIR spectra of $Fe_2O_3$/biochar. $Fe_2O_3$/biochar spectra show a broad peak at 3374 $cm^{-1}$ ascribed to –OH groups. Furthermore, the peak at 1589 $cm^{-1}$ recognize to vibration of C=C and at 1059 $cm^{-1}$ is corresponding C–O vibration.[44] Finally, the peak centered at 611 $cm^{-1}$ is assigned to Fe–O vibrations. The same results were reported in the literature for the synthesis of magnetic Fe/AC nanocomposites.[45] The Raman spectrum of $Fe_2O_3$/biochar is shown in Fig. 1c. For

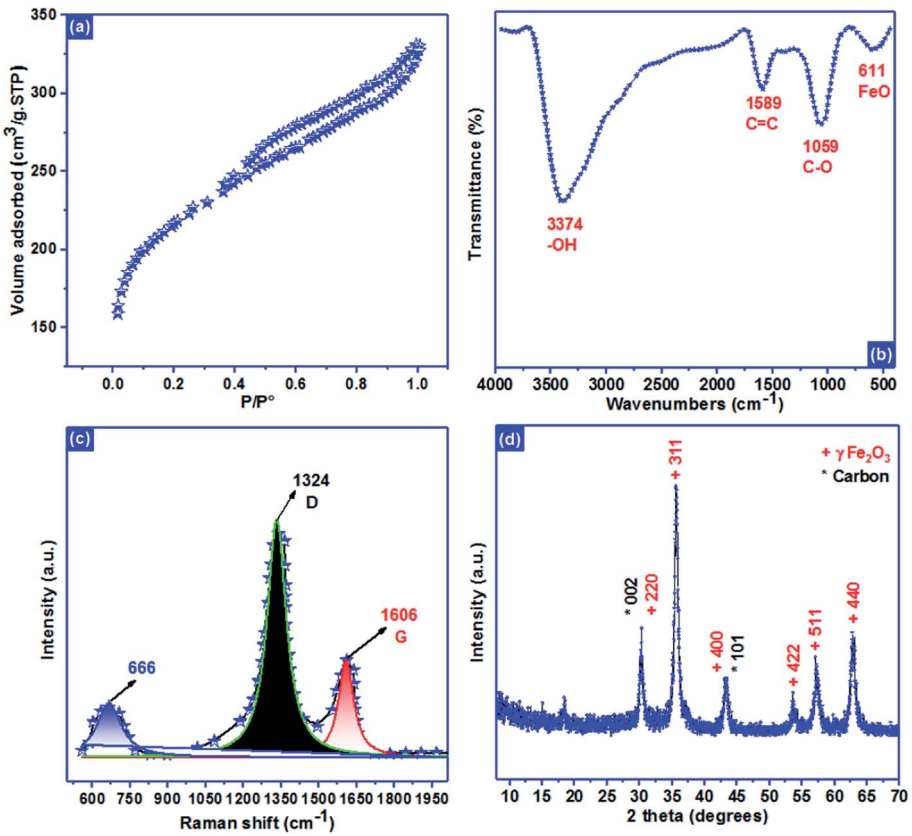


Fig. 1 (a) $N_2$ adsorption–desorption, (b) Fourier transform infrared spectrometry, (c) Raman spectrometry and (d) X-ray diffraction.

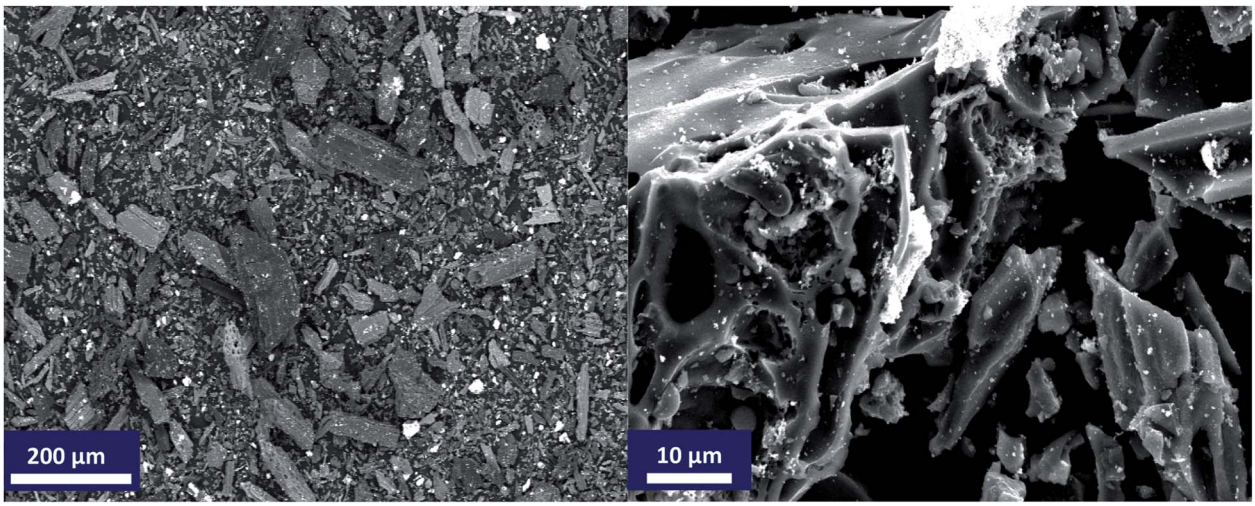


Fig. 2 Scanning electron microscopy of $Fe_2O_3$/biochar.

$Fe_2O_3$/biochar, the peak located at 666 $cm^{-1}$ is assigned to the $A_{1g}$ modes of Fe.[46] Moreover, the G peak at 1606 $cm^{-1}$ is related to $E_{2g}$ graphite mode and D-line at ~1324 $cm^{-1}$ is induced by defective structures.[47] Fig. 1d displays XRD patterns of $Fe_2O_3$/biochar. The diffraction pattern of $Fe_2O_3$/biochar confirms that iron oxide present in biochar is corresponding with the standard γ-Fe structure (JCPDS no. 39-1346). Moreover, the formation of γ-$Fe_2O_3$ phase was also confirmed by Raman analysis (Fig. 1d). Fig. 2 display the SEM micrographs of prepared $Fe_2O_3$/biochar. The particle of Fe can be clearly seen on the surface, this confirmed the successful impregnation. As well, the heterogeneous and porous surface was clearly observed which developed after pyrolysis. The EDS analysis (Table 2) indicate the presence of three main atoms: carbon (68.75%), oxygen (23.37%), and Fe (7.23%). EDS analysis of $Fe_2O_3$/biochar showed many other chemicals elements as Al, P, S and Ca. The magnetic properties of prepared composite were analyzed at room temperature by using MPMS-XL-7A. Magnetic hysteresis loop show that the saturation magnetic moment was equal 0.0036 emu $g^{-1}$ (Fig. 3). This small saturation magnetic moment was attributed to the mass of biochar in magnetic nanocomposites, which does not contribute to the magnetic moment as which was consistent with the published results.[48]

Table 2 $Fe_2O_3$/biochar chemicals elements determined by EDS analysis

| Element | Line s. | Mass (%) | Mass norm. (%) | Atom (%) |
|---|---|---|---|---|
| C | K-serie | 74.63 | 50.77 | 68.75 |
| O | K-serie | 33.79 | 22.99 | 23.37 |
| Al | K-serie | 0.12 | 0.08 | 0.05 |
| P | K-serie | 0.03 | 0.02 | 0.01 |
| S | K-serie | 0.88 | 0.60 | 0.31 |
| Ca | K-serie | 1.07 | 0.73 | 0.29 |
| Fe | K-serie | 36.48 | 24.82 | 7.23 |
| | | 147.00 | 100.00 | 100.00 |

### 3.2. Adsorption performance

**3.2.1. Effect of pH.** The $pH_{PZC}$ is the main key that governs the type of charges on the surface of an adsorbent. $Fe_2O_3$/biochar has a $pH_{PZC}$ of 6.73, as shown in Fig. 4b. Consequently, the surface of $Fe_2O_3$/biochar has positive charges at pH < 6.73 and negative charges at pH > 6.73. Fig. 4a displays the effect of solution pH (2–12) with an initial concentration of 100 mg $L^{-1}$ on $Fe_2O_3$/biochar performance towards SA, Nap, and Keto removal. The initial pH played an essential role in SA, Nap, and Keto adsorption on $Fe_2O_3$/biochar. The removal of SA, Nap, and Keto was higher in acidic solutions than in the basic medium. The high removal of SA (99.52%), Nap (95.86%), and Keto (93.45%) were observed at pH 3.2. At pH 3.2, the SA, Nap, and Keto molecules are in their neutral forms.[49–52] They can form strong H-bonds with oxygen-containing surface functional groups present in the surface of $Fe_2O_3$/biochar and be not

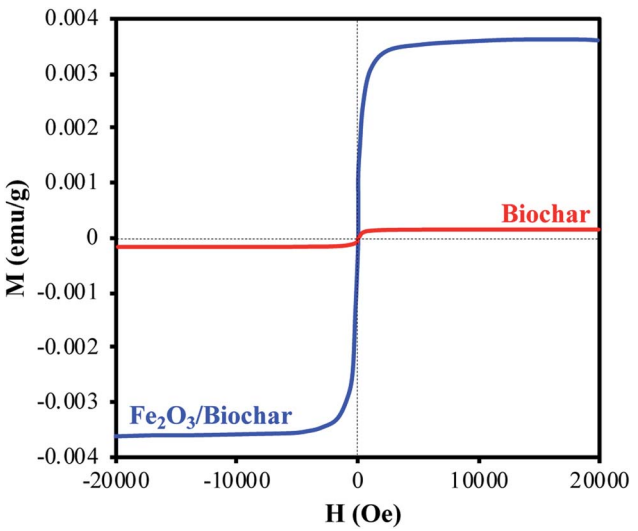


Fig. 3 Magnetic hysteresis loop of biochar and $Fe_2O_3$/biochar composite.

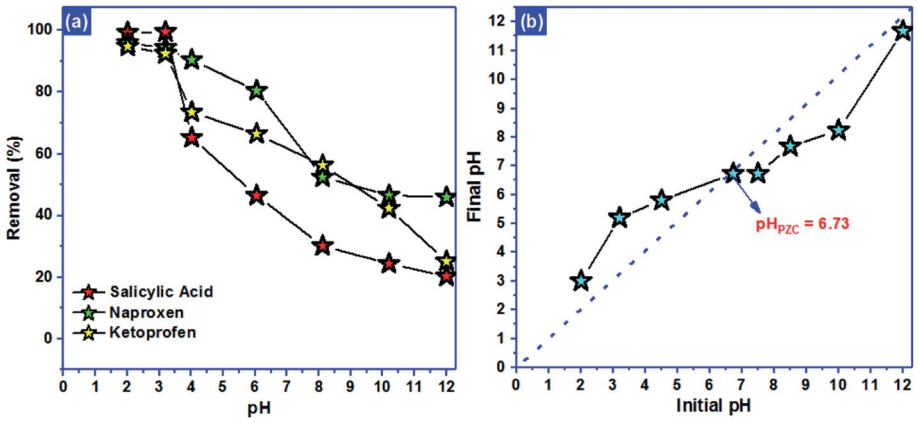


Fig. 4 (a) The $pH_{PZC}$ of $Fe_2O_3$/biochar and (b) effect of pH solution.

Table 3 Concentrations (meq. $g^{-1}$) of acidic and basic surface groups of prepared composites

| | Total acidity (meq. $g^{-1}$) | Total basicity (meq. $g^{-1}$) |
|---|---|---|
| Biochar/$Fe_2O_3$ | 4.13 | 4.76 |

repelled by the surface positive charge.[53] Accordingly, they revealed their maximum removal at pH 3.2. The increases in solution pH from 3.2 to 12, SA molecules were changed to its carboxylate conjugate bases, which was repelled from the increasingly negatively charged $Fe_2O_3$/biochar surfaces. Hence, the removal of SA, Nap, and Keto in molecular form was favorable to the $Fe_2O_3$/biochar, while the adsorption of the anionic form of SA, Nap, and Keto was unfavorable.[49–52,54] In addition, the acidic and basic surface functions of the prepared adsorbent were determined according to the Boehm. Thus, 0.5 g of the powder was mixed with 50 mL of one of the three bases solutions $NaHCO_3$ (0.05 M), $Na_2CO_3$ (0.05 M) and NaOH (0.05 M) to identify the organic acid surface groups (–COOH), (–COO–) and (–OH), respectively, as described elsewhere.[55] The

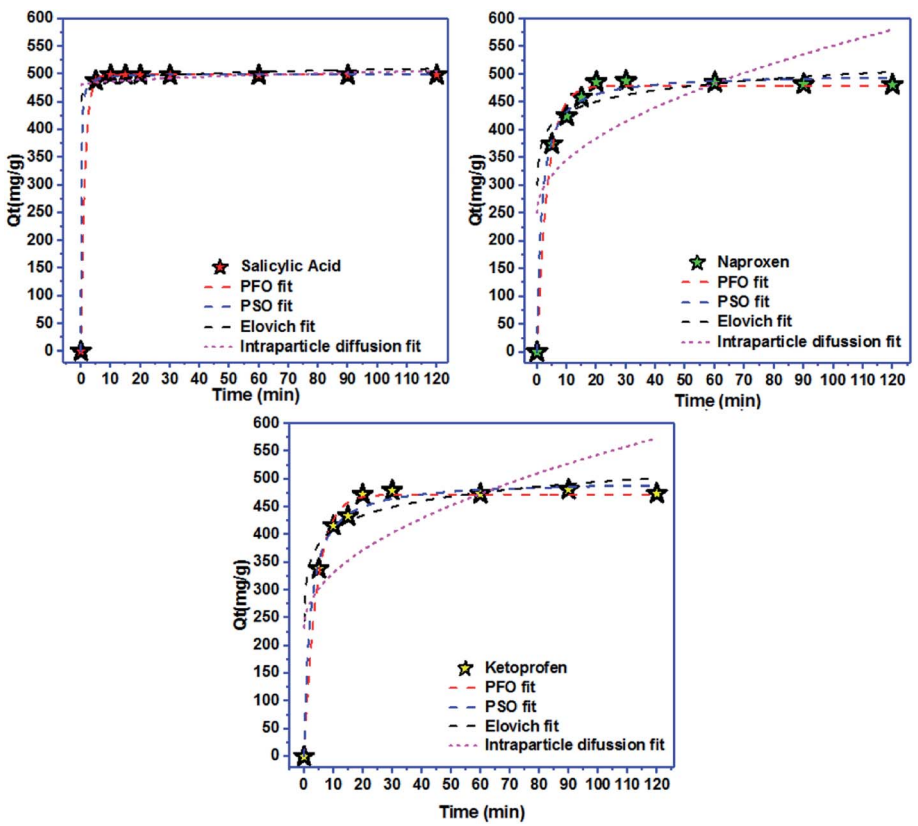


Fig. 5 Effect of contact time and adsorption kinetics for salicylic acid, naproxen, and ketoprofen removal.

Table 4 Kinetics adsorption parameters

| | Pseudo-first-order model | | | | Pseudo-second-order model | | |
|---|---|---|---|---|---|---|---|
| | $Q_{e,exp}$ (mg g$^{-1}$) | $Q_{e,cal}$ (mg g$^{-1}$) | $K_1$ (min$^{-1}$) | $R^2$ | $Q_{e,cal}$ (mg g$^{-1}$) | $K_2$ (g mg$^{-1}$ min$^{-1}$) | $R^2$ |
| Salicylic acid | **498.97** | 498.92 | 0.76 | 1.000 | 500.73 | 0.018 | 0.998 |
| Naproxen | **481.38** | 479.80 | 0.27 | 0.994 | 500.69 | 0.001 | 0.991 |
| Ketoprofen | **473.13** | 472.26 | 0.23 | 0.994 | 497.47 | 0.001 | 0.992 |

| | Elovich model | | | Intra-particle diffusion model | | |
|---|---|---|---|---|---|---|
| | $\alpha$ (mg g$^{-1}$ min$^{-1}$) | $B$ (g mg$^{-1}$) | $R^2$ | $K_{ip}$ | $C$ | $R^2$ |
| Salicylic acid | 4.47 | 0.12 | 0.978 | 2.39 | 480.24 | 0.097 |
| Naproxen | 6.42 | 0.03 | 0.979 | 30.12 | 250.37 | 0.455 |
| Ketoprofen | 2.13 | 0.03 | 0.972 | 31.10 | 232.69 | 0.499 |

results of pH effect consistent with the results of Boehm's titration. In fact, the high concentration of basic functions favors attractive electrostatic interaction occurring between molecules and the adsorbent surface (Table 3).

**3.2.2. Effect of contact time and adsorption kinetics.** Pseudo-first-order kinetic, pseudo-second-order kinetic and Elovich models have been applied to analyze the experimental data of SA, Nap, and Keto removal onto $Fe_2O_3$/biochar.[44,56] The adsorption capacity for all molecules increased gradually with the increase in contact time. The rate of adsorption SA, Nap, and Keto removal was rapid in the beginning due to availability of vacant sites and active functional groups on the surface of $Fe_2O_3$/biochar (Fig. 5). The kinetic parameters are presented in Table 4 using non-linear regression analysis. The values of rate constants ($k_1$ and $k_2$) and regression coefficient ($R^2$) shows that the pseudo-second order kinetic model represents the adsorption of SA, Nap, and Keto removal onto $Fe_2O_3$/biochar in comparison to pseudo-first-order model and Elovich. In

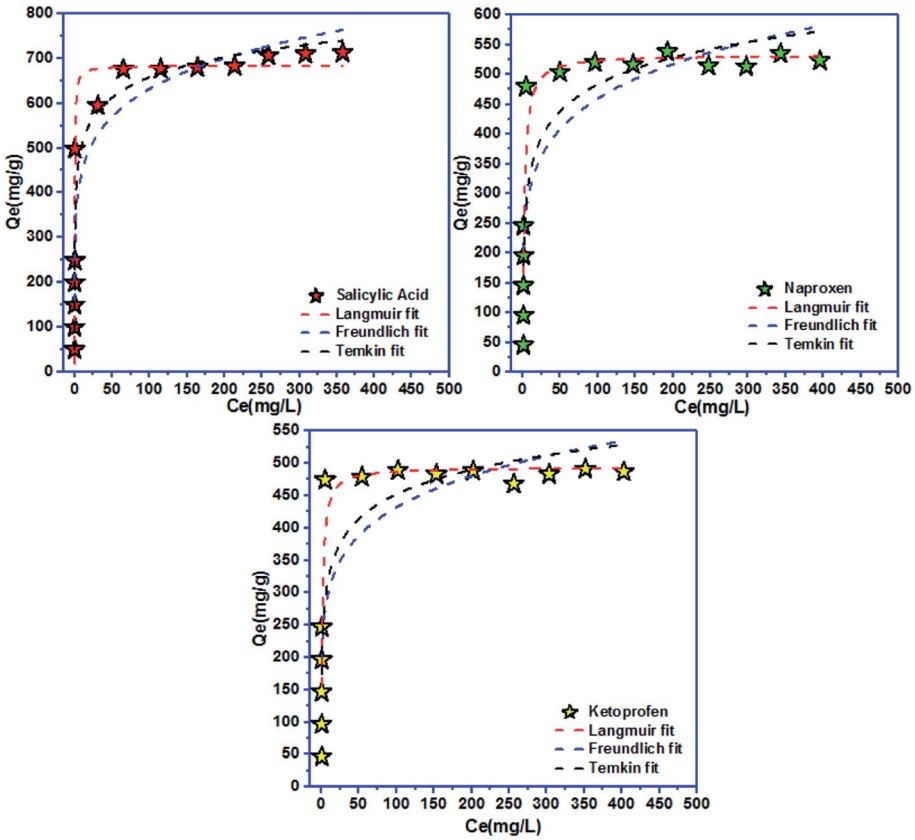


Fig. 6 Langmuir, Freundlich, and Temkin models for salicylic acid, naproxen, and ketoprofen removal at equilibrium.

 

Table 5 Equilibrium adsorption parameters of salicylic acid, naproxen, and ketoprofen removal

| | Langmuir isotherm | | | | Freundlich isotherm | | |
|---|---|---|---|---|---|---|---|
| | $Q_{max}$ (mg g$^{-1}$) | $K_L$ (L mg$^{-1}$) | $R_L$ | $R^2$ | $K_F$ ((mg g$^{-1}$)/(mg L$^{-1}$)$^n$) | $n$ | $R^2$ |
| Salicylic acid | **683** | 3.44 | 0.006 | 0.977 | 318.83 | 6.73 | 0.900 |
| Naproxen | **533** | 0.50 | 0.004 | 0.912 | 210 | 5.88 | 0.766 |
| Ketoprofen | **494** | 0.71 | 0.003 | 0.914 | 212 | 6.49 | 0.754 |

| | Temkin isotherm | | |
|---|---|---|---|
| | $B_T$ (J mol$^{-1}$) | $K_T$ (L g$^{-1}$) | $R^2$ |
| Salicylic acid | 0.015 | 268.59 | 0.945 |
| Naproxen | 0.015 | 18.24 | 0.823 |
| Ketoprofen | 0.018 | 37.04 | 0.796 |

addition, close agreement was observed between experimental and theoretical values of adsorption capacity using this model. The intra-particle model was not the main controlling step during SA, Nap, and Keto removal onto $Fe_2O_3$/biochar.

**3.2.3. Adsorption isotherms.** To establish equilibrium between SA, Nap, and Keto removal onto $Fe_2O_3$/biochar Langmuir, Freundlich, and Temkin models were used.[41,57] The initial SA, Nap and Keto concentration was varied from 100 to 500 mg L$^{-1}$ at a constant temperature (Fig. 6). The nonlinear isotherms plot of SA, Nap, and Keto adsorption onto $Fe_2O_3$/biochar showed that the Langmuir isotherm (homogeneous distribution of active sites on the adsorbent surface[58]) was the best applicable model to explain the data based on $R^2$, which is higher compared to $R^2$ of Freundlich and Temkin. The calculated values for Langmuir, Freundlich, and Temkin parameters were summarized in Table 5. The maximum adsorption capacities $Q_{max}$ of SA, Nap, and Keto were equal to 683 mg g$^{-1}$, 533 mg g$^{-1}$, and 444 mg g$^{-1}$, respectively. The values of $R_L$ and Freundlich constant $n$ are investigated to explain the nature of the adsorption process. The SA, Nap, and Keto adsorption was favorable because $R_L$ between 0 and 1, and $1/n$ parameter was smaller than 1.[56] The sorption capacity values obtained from various adsorbents reported in the literature were listed in Table 6 and shows that the $Fe_2O_3$/biochar are comparable with those reported in the literature and showed better results.

### 3.3. Renewability, mechanism and thermodynamic behavior

Renewability is an important factor to evaluate the adsorbent pollutants adsorption.[64,65] The $Fe_2O_3$/biochar regenerated was investigated using ethanol for 4 hours of stirring. The sorption regeneration was repeated 5 times for SA, Nap, and Keto molecules (Fig. 7a). After 5 cycles, the performance sorption decreased from:[65]

99.52% → 97.16%, 95.86% → 94.30% and 93.45% → 92.01% for SA, Nap, and Keto molecules, respectively. The sorption regeneration test revealed that the $Fe_2O_3$/biochar could be effectively used as a promising adsorbent for SA, Nap, and Keto nonsteroidal molecules adsorption from aqueous solutions.

The ultrasound-assisted adsorption mechanism of NSAIDs (salicylic acid, naproxen, and ketoprofen) onto $Fe_2O_3$/biochar was investigated using FTIR after adsorption (Fig. 7b). The fixation of anti-inflammatory pharmaceuticals pollutants molecules inside the adsorbent pores was not only the determined step of process adsorption. FTIR analysis after adsorption shows that the peaks of –OH groups, carbon–carbon bond with sp$^2$ hybridization, C–O vibration, and Fe–O vibrations were shifted from the original position. These results confirm that the mechanism of adsorption referred to the formation of hydrogen bonding, the π–π interaction between, an electrostatic attraction with C–O groups and the interaction between Keto molecules and Fe impregnated on the biochar surface.

Thermodynamic parameters offer extra deep information about the inherent energetic changes involved during adsorption. To evaluate the thermodynamic parameters, the adsorption isotherms of SA, Nap, and Keto on $Fe_2O_3$/biochar surfaces were measured at 293 K, 303 K and 313 K and changes in thermodynamic parameters of the standard Gibbs free energy of adsorption $\Delta G^\circ$, the standard enthalpy $\Delta H^\circ$ and the standard entropy $\Delta S^\circ$ were calculated using Van't Hoff and Gibbs free energy equations presented in Table 7. The $R^2$ value is higher

Table 6 Adsorption capacities compared to the literature data

| | Adsorbent | $Q_{max}$ (mg g$^{-1}$) | Reference |
|---|---|---|---|
| Salicylic acid | $Fe_2O_3$/biochar | **683** | **This work** |
| | Barley straw biochar | 210 | 54 |
| | Cross-linked resin | 396 | 59 |
| | Douglas fir biochar | 108 | 60 |
| Naproxen | $Fe_2O_3$/biochar | **533** | **This work** |
| | ED-MIL-101 | 154 | 50 |
| | MIL-101-$(OH)_3$ | 156 | 61 |
| | Oxidized activated carbon | 80 | 51 |
| | Activated carbon | 39 | 51 |
| Ketoprofen | $Fe_2O_3$/biochar | **494** | **This work** |
| | Activated carbon | 25 | 62 |
| | MIL-101-$(OH)_3$ | 80 | 61 |
| | Graphene oxide | 63 | 63 |
| | MIL-101(Cr)/CS | 156 | 52 |

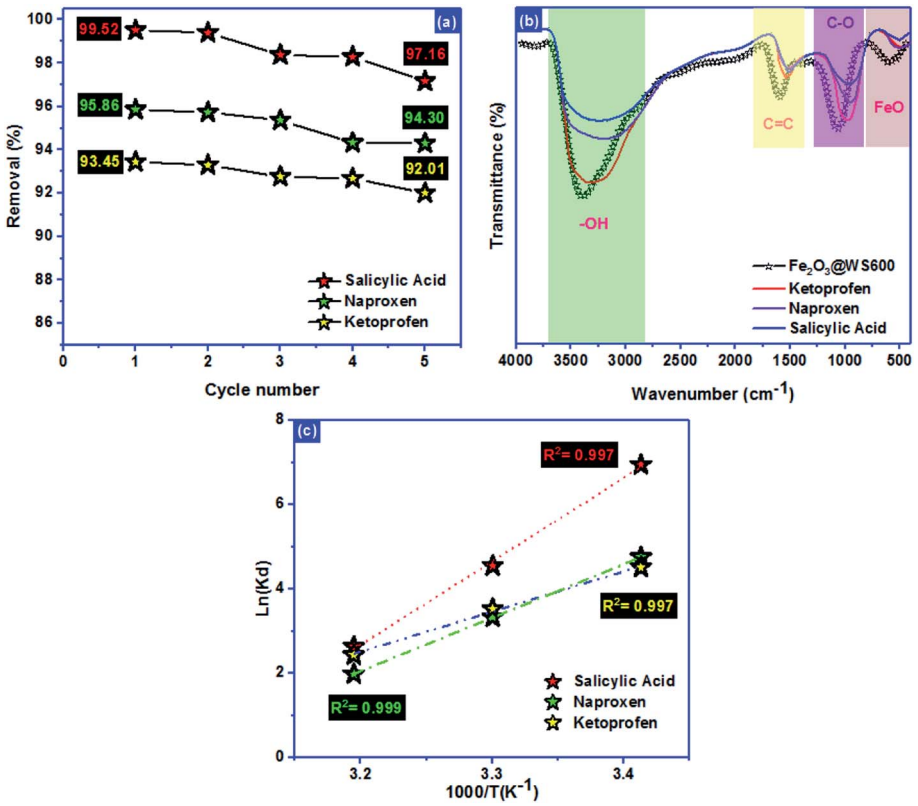


Fig. 7 (a) Renewability, (b) mechanism and (c) thermodynamic behavior of salicylic acid, naproxen, and ketoprofen adsorption.

than 0.99, indicating that the SA, Nap, and Keto adsorption data fitted well the Van't Hoff equation (Fig. 7c).

The negative $\Delta H^\circ$ (SA: −164.51 J mol$^{-1}$; Nap: −105.50 J mol$^{-1}$; Keto: −79.51 J mol$^{-1}$) affirmed the exothermic nature of SA, Nap, and Keto adsorption on $Fe_2O_3$/biochar (Table 7). The negative $\Delta S^\circ$ (SA: −504.22 J mol$^{-1}$; Nap: −320.56 J mol$^{-1}$; Keto: −233.58 J mol$^{-1}$) revealed the decreases randomness solid/liquid interface during adsorption process (Table 7). If the heat value of adsorption process ranges from 40 kJ mol$^{-1}$ to 800 kJ mol$^{-1}$, the adsorption process is typically chemisorption, while the values less than 40 kJ mol$^{-1}$ denote to a physisorption process.[20] In this study, the heat of SA, Nap, and Keto adsorption on $Fe_2O_3$/biochar were less than 40 kJ mol$^{-1}$, which indicate that the process was predominantly a physical adsorption. The Gibbs free energy change $\Delta G^\circ$ reveals the possibility of the adsorption process of SA, Nap, and Keto on $Fe_2O_3$/biochar. The $\Delta G^\circ$ values were negative at all temperatures, proving that the adsorption of SA, Nap, and Keto was spontaneous and thermodynamically favorable.

Table 7 Thermodynamic parameters of salicylic acid, naproxen, and ketoprofen adsorption

| | $\Delta H$ (J mol$^{-1}$) | $\Delta S$ (J mol$^{-1}$ K$^{-1}$) | $\Delta G$ (kJ mol$^{-1}$) | | |
|---|---|---|---|---|---|
| | | | 293 K | 303 K | 313 K |
| Salicylic acid | −164.51 | −504.22 | −16.91 | −10.88 | −6.84 |
| Naproxen | −105.50 | −320.56 | −11.57 | −8.37 | −5.16 |
| Ketoprofen | −79.51 | −233.58 | −11.00 | −8.88 | −6.31 |

## 4 Conclusion

The present study evaluated the ultrasound-assisted adsorption capacity of salicylic acid, naproxen and ketoprofen (SA, Nap, and Keto) onto $Fe_2O_3$/biochar prepared by green synthesis *via* microwave. The results revealed that the sorption was dependent on different functional parameters such as pH, temperature, contact time and concentration. The characteristics of prepared material predicted several functional groups on the surfaces and shows very interesting textural and morphological properties. Results show that the removal of SA, Nap, and Keto were higher in the acidic medium than in the basic medium. The adsorption kinetics and isotherms were well fitted to the pseudo-second-order model and Langmuir for all adsorbates. The maximum adsorption capacities reached 683, 533 and 444 mg g$^{-1}$ for SA, Nap, and Keto, respectively. The thermodynamic study from the experimental model showed that all $\Delta G^\circ$, $\Delta H^\circ$ and $\Delta S^\circ$ parameters values are negative, indicating that the adsorption was exothermic, spontaneous and thermodynamically favorable. The thermodynamic study showed that the heat was less than 40 kJ mol$^{-1}$, which indicate that the process was predominantly a physical adsorption, involving hydrogen bond type interaction, the π–π interaction and electrostatic attraction with surface functional groups. $Fe_2O_3$/biochar could potentially be applied as an

 

efficient adsorbent for the removal of SA, Nap, and Keto from aqueous solutions.

## Conflicts of interest

The authors declare that they do not have any conflict of interest.

## References

1 K. Fent, A. A. Weston and D. Caminada, *Aquat. Toxicol.*, 2006, **76**, 122–159.
2 T. Heberer, *Toxicol. Lett.*, 2002, **131**, 5–17.
3 D. F. Martin, J. M. Martin and T. A. Ward, *J. Environ. Sci. Health, Part A: Toxic/Hazard. Subst. Environ. Eng.*, 2016, **51**, 186–191.
4 T. Kosjek, E. Heath and A. Krbavčič, *Environ. Int.*, 2005, **31**, 679–685.
5 A. Togola and H. Budzinski, *J. Chromatogr. A*, 2008, **1177**, 150–158.
6 M. D. Hernando, E. Heath, M. Petrovic and D. Barceló, *Anal. Bioanal. Chem.*, 2006, **385**, 985–991.
7 D. Zhang, R. M. Gersberg, W. J. Ng and S. K. Tan, *Environ. Pollut.*, 2014, **184**, 620–639.
8 H. F. D. Almeida, I. M. Marrucho and M. G. Freire, *ACS Sustainable Chem. Eng.*, 2017, **5**, 2428–2436.
9 V. Rakić, V. Rac, M. Krmar, O. Otman and A. Auroux, *J. Hazard. Mater.*, 2015, **282**, 141–149.
10 Y. Zhou, X. Liu, Y. Xiang, P. Wang, J. Zhang, F. Zhang, J. Wei, L. Luo, M. Lei and L. Tang, *Bioresour. Technol.*, 2017, **245**, 266–273.
11 Y. Zhou, X. Liu, L. Tang, F. Zhang, G. Zeng, X. Peng, L. Luo, Y. Deng, Y. Pang and J. Zhang, *J. Hazard. Mater.*, 2017, **333**, 80–87.
12 S. E. Evans, P. Davies, A. Lubben and B. Kasprzyk-Hordern, *Anal. Chim. Acta*, 2015, **882**, 112–126.
13 F. Sopaj, M. A. Rodrigo, N. Oturan, F. I. Podvorica, J. Pinson and M. A. Oturan, *Chem. Eng. J.*, 2015, **262**, 286–294.
14 X. Liu, D. Yang, Y. Zhou, J. Zhang, L. Luo, S. Meng, S. Chen, M. Tan, Z. Li and L. Tang, *Chemosphere*, 2017, **182**, 306–315.
15 D. Russo, A. Siciliano, M. Guida, E. Galdiero, A. Amoresano, R. Andreozzi, N. M. Reis, G. Li Puma and R. Marotta, *Water Res.*, 2017, **122**, 591–602.
16 F. Méndez-Arriaga, R. A. Torres-Palma, C. Pétrier, S. Esplugas, J. Gimenez and C. Pulgarin, *Water Res.*, 2008, **42**, 4243–4248.
17 E. Isarain-Chávez, R. M. Rodríguez, P. L. Cabot, F. Centellas, C. Arias, J. A. Garrido and E. Brillas, *Water Res.*, 2011, **45**, 4119–4130.
18 S. A. Baig, T. Sheng, C. Sun, X. Xue, L. Tan and X. Xu, *PLoS One*, 2014, **9**, e100704.
19 G. Zelmanov and R. Semiat, *Desalination*, 2014, **333**, 107–117.
20 M. Zbair, K. Ainassaari, A. Drif, S. Ojala, M. Bottlinger, M. Pirilä, R. L. Keiski, M. Bensitel and R. Brahmi, *Environ. Sci. Pollut. Res.*, 2018, **25**, 1869–1882.
21 I. Anastopoulos, A. Bhatnagar, B. Hameed, Y. S. Ok and M. Omirou, A review on waste-derived adsorbents from sugar industry for pollutant removal in water and wastewater, *J. Mol. Liq.*, 2017, **240**, 179–188.
22 M. Zbair, Z. Anfar, H. Khallok and H. A. Ahsaine, *Fullerenes, Nanotubes, Carbon Nanostruct.*, 2018, **26**, 433–442.
23 Z. Anfar, A. Amedlous, A. Ait El Fakir, H. Ait Ahsaine, M. Zbair, S. Lhanafi, R. El Haouti, A. Jada and N. El Alem, *ACS Omega*, 2019, **4**, 9434–9445.
24 Z. Anfar, M. Zbair, H. A. Ahsaine, Y. Abdellaoui, A. A. El Fakir, E. H. Amaterz, A. Jada and N. El Alem, *ChemistrySelect*, 2019, **4**, 4981–4994.
25 Z. Anfar, H. Ait Ahsaine, M. Zbair, A. Amedlous, A. Ait El Fakir, A. Jada and N. El Alem, *Crit. Rev. Environ. Sci. Technol.*, 2019, 1–42.
26 H. Li, D. Zhang, X. Han and B. Xing, *Chemosphere*, 2014, **95**, 150–155.
27 B. Huang, Y. Liu, B. Li, S. Liu, G. Zeng, Z. Zeng, X. Wang, Q. Ning, B. Zheng and C. Yang, *Carbohydr. Polym.*, 2017, **157**, 576–585.
28 C. Ling, X. Li, Z. Zhang, F. Liu, Y. Deng, X. Zhang, A. Li, L. He and B. Xing, *Environ. Sci. Technol.*, 2016, **50**, 10015–10023.
29 D. Mohan, A. Sarswat, Y. S. Ok and C. U. Pittman, *Bioresour. Technol.*, 2014, **160**, 191–202.
30 B. Wang, Y. Jiang, F. Li and D. Yang, *Bioresour. Technol.*, 2017, **233**, 159–165.
31 C. Gan, Y. Liu, X. Tan, S. Wang, G. Zeng, B. Zheng, T. Li, Z. Jiang and W. Liu, *RSC Adv.*, 2015, **5**, 35107–35115.
32 H. A. Ahsaine, M. Zbair and R. El Haouti, *Desalin. Water Treat.*, 2017, **85**, 330–338.
33 X. Tan, S. Liu, Y. Liu, Y. Gu, G. Zeng, X. Cai, Z. Yan, C. Yang, X. Hu and B. Chen, *Sci. Rep.*, 2016, **6**, 39691.
34 Y. Ma, W.-J. Liu, N. Zhang, Y.-S. Li, H. Jiang and G.-P. Sheng, *Bioresour. Technol.*, 2014, **169**, 403–408.
35 X. Huang, Y. Liu, S. Liu, X. Tan, Y. Ding, G. Zeng, Y. Zhou, M. Zhang, S. Wang and B. Zheng, *RSC Adv.*, 2016, **6**, 94–104.
36 J. Wang, C. P. Huang, H. E. Allen, D. K. Cha and D. W. Kim, *J. Colloid Interface Sci.*, 1998, **208**, 518–528.
37 V. K. Garg, R. Gupta, A. B. Yadav and R. Kumar, *Bioresour. Technol.*, 2003, **89**, 121–124.
38 B. K. S. Lagergren, *Z. Chem. Ind. Kolloide*, 1898, **24**, 15.
39 G. McKay, *Process Biochem.*, 1999, **34**, 451.
40 W. J. Weber and J. C. Morris, *J. Sanit. Eng. Div. Proc. Am. Soc. Civ. Eng.*, 1963, **89**, 31–60.
41 I. Langmuir, *J. Am. Chem. Soc.*, 1916, **38**, 2221–2295.
42 H. Freundlich, *Z. Phys. Chem.*, 1907, **57U**(1), 385–470.
43 M. Thommes, K. Kaneko, A. V. Neimark, J. P. Olivier, F. Rodriguez-Reinoso, J. Rouquerol and K. S. W. Sing, *Pure Appl. Chem.*, 2015, **87**, 1051–1069.
44 M. Zbair, Z. Anfar, H. Ait Ahsaine, N. El Alem and M. Ezahri, *J. Environ. Manage.*, 2018, **206**, 383–397.
45 R.-S. Juang, Y.-C. Yei, C.-S. Liao, K.-S. Lin, H.-C. Lu, S.-F. Wang and A.-C. Sun, *J. Taiwan Inst. Chem. Eng.*, 2018, **90**, 51–60.
46 A. M. Jubb and H. C. Allen, *ACS Appl. Mater. Interfaces*, 2010, **2**, 2804–2812.

47 H. Ait Ahsaine, M. Zbair, Z. Anfar, Y. Naciri, R. El haouti, N. El Alem and M. Ezahri, *Mater. Today Chem.*, 2018, **8**, 121–132.
48 Y. Zhang, M. Z. Joel, Y. He, D. Weathersby, F. Han, G. Rimal, J. Tang and Q. Dai, *Materials Letters: X*, 2019, **3**, 100020.
49 V. Bernal, L. Giraldo and J. C. Moreno-Piraján, *Adsorpt. Sci. Technol.*, 2017, **36**, 833–850.
50 Z. Hasan, E. J. Choi and S. H. Jhung, *Chem. Eng. J.*, 2013, **219**, 537–544.
51 J. Y. Song, B. N. Bhadra and S. H. Jhung, *Microporous Mesoporous Mater.*, 2017, **243**, 221–228.
52 N. Zhuo, Y. Lan, W. Yang, Z. Yang, X. Li, X. Zhou, Y. Liu, J. Shen and X. Zhang, *Sep. Purif. Technol.*, 2017, **177**, 272–280.
53 X. Ling, H. Li, H. Zha, C. He and J. Huang, *Chem. Eng. J.*, 2016, **286**, 400–407.
54 M. J. Ahmed and B. H. Hameed, *J. Cleaner Prod.*, 2018, **195**, 1162–1169.
55 A. M. Oickle, S. L. Goertzen, K. R. Hopper, Y. O. Abdalla and H. A. Andreas, *Carbon*, 2010, **48**, 3313–3322.
56 Z. Anfar, R. El Haouti, S. Lhanafi, M. Benafqir, Y. Azougarh and N. El Alem, *J. Environ. Chem. Eng.*, 2017, **5**, 5857–5867.
57 H. M. F. Freundlich, *J. Phys. Chem.*, 1906, **57**, 385–471.
58 L. Wang, J. Zhang, R. Zhao, Y. Li, C. Li and C. Zhang, *Bioresour. Technol.*, 2010, **101**, 5808–5814.
59 G. Xiao, R. Wen, A. Liu, G. He and D. Wu, *J. Hazard. Mater.*, 2017, **329**, 77–83.
60 A. G. Karunanayake, O. A. Todd, M. L. Crowley, L. B. Ricchetti, C. U. Pittman, R. Anderson and T. E. Mlsna, *Chem. Eng. J.*, 2017, **319**, 75–88.
61 J. Y. Song and S. H. Jhung, *Chem. Eng. J.*, 2017, **322**, 366–374.
62 R. Baccar, M. Sarrà, J. Bouzid, M. Feki and P. Blánquez, *Chem. Eng. J.*, 2012, **211–212**, 310–317.
63 F. Liu, J. Zhao, S. Wang, P. Du and B. Xing, *Environ. Sci. Technol.*, 2014, **48**, 13197–13206.
64 Z. Anfar, M. Zbair, H. A. Ahsaine, M. Ezahri and N. El Alem, *Fullerenes, Nanotubes, Carbon Nanostruct.*, 2018, **26**, 389–397.
65 H. Ait Ahsaine, Z. Anfar, M. Zbair, M. Ezahri and N. El Alem, *J. Chem.*, 2018, **2018**, DOI: 10.1155/2018/6982014.

 